Cosmic Silicates

Thomas Henning

Max Planck Institute for Astronomy, D-69117 Heidelberg, Germany;
email: henning@mpia-hd.mpg.de

Annu. Rev. Astron. Astrophys. 2010. 48:21–46

First published online as a Review in Advance on March 23, 2010

The *Annual Review of Astronomy and Astrophysics* is online at astro.annualreviews.org

This article's doi:
10.1146/annurev-astro-081309-130815

0066-4146/10/0922-0021$20.00

Key Words

infrared (IR) astronomy, interstellar grains, cosmic dust

Abstract

Silicate dust particles are an important player in the cosmic life cycle of matter. They have been detected in a wide variety of environments, ranging from nearby protoplanetary disks to distant quasars. This review summarizes the fundamental properties of silicates relevant to astronomical observations and processes. It provides a review of our knowledge about cosmic silicates, mostly based on results from IR spectroscopy.

1. INTRODUCTION

Silicates are an important ingredient of the cosmic life cycle of matter. They freshly form in the winds of AGB stars; get modified, destroyed, and potentially reformed in the diffuse ISM; and are an important dust component of protoplanetary and debris disks. As part of the general interstellar and circumstellar dust populations, silicates regulate the thermal structure of the dense and cold phases of these media and provide the surface for chemical reactions. Silicate dust grains contribute to the interstellar extinction and emit thermal radiation at IR and millimeter wavelengths. Their mid-IR spectral features have important diagnostic value for constraining both the chemical composition of dust and the size of grains. The analysis of these features provides information about the thermal and density structure of circumstellar disks and envelopes and the toroidal structures around AGNs.

Based on IR spectroscopy, cosmic silicates have been identified in very diverse environments, ranging from objects in the Solar System to luminous quasars. The crust of our planet is mainly in the form of silicates, occurring as silicate rocks. The main building blocks of cosmic silicates are the abundant elements O, Si, Fe, and Mg, and to a lesser degree Ca and Al.

Cosmic silicates have been mostly found in amorphous state, characterized by broad and structureless IR bands at 10 and 18 μm that can be attributed to Si–O stretching and O–Si–O bending modes, respectively. These bands were first seen in the IR spectra of M giants and supergiants and identified with silicates as their carriers (Woolf & Ney 1969). In circumstellar environments, both around (post-)AGB stars and in disks around Herbig Ae/Be stars, T Tauri stars, and brown dwarfs, evidence for crystalline silicates has been found through a forest of sharp solid-state features. These "fingerprint" spectra make the identification of silicate minerals in space possible. For an early summary of the evidence for crystalline silicates in circumstellar environments around stars, we refer to Molster & Waters (2003). This review mainly concentrates on the properties of silicates outside of the Solar System where the main information source is IR spectroscopy. For reviews dealing with silicates in cometary environments, we refer to Wooden (2008), Kelley & Wooden (2009), and Hanner & Zolensky (2010). Silicate spectra from asteroids are discussed by Feierberg, Witteborn & Lebofsky (1983) and Emery, Cruikshank & van Cleve (2006). The mineralogy of interplanetary dust particles is summarized by Bradley (2010). In this context, we also refer to the book *Astromineralogy* for a broader discussion of minerals in space (Henning 2003, 2010).

In this review we provide a summary of the basic properties of silicates and their characterization through laboratory experiments. Such experimental data usually form the basis for the interpretation of astronomical spectra.

Owing to the vast amount of studies dealing with cosmic silicates, especially in the context of the *Spitzer Infrared Telescope* (*Spitzer*), we are not able to refer to all "silicate" papers and only provide exemplary references where more literature can be found. For a discussion of silicates in the general context of interstellar dust, we refer to the reviews by Dorschner & Henning (1995) and Draine (2003).

2. SILICATES: BASIC PROPERTIES

2.1. Structural Properties

Silicates form a class of materials with a large diversity in chemical composition and structural properties (Liebau 1985, Colangeli et al. 2003). With the exception of high-pressure modifications, the Si atoms are invariably coordinated in a tetrahedron by four O atoms (see **Figure 1**). The different silicate structures are produced by linking individual $[SiO_4]^{4-}$ tetrahedra in various levels

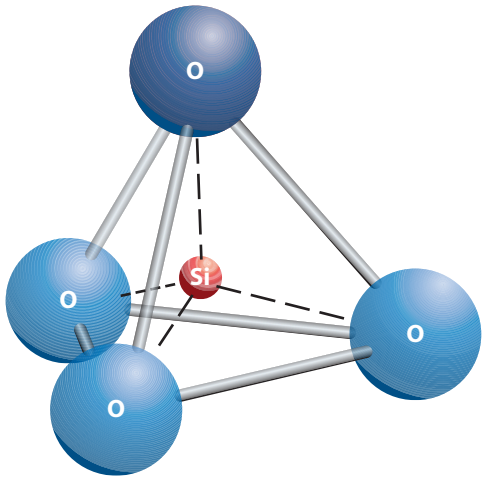

Figure 1

A SiO_4 tetrahedron as the basic structural unit of silicates. The silicon (*red sphere*) sits in the center of the structure and is surrounded by four oxygen atoms (*blue spheres*).

of complexity. These different states of polymerization can range from isolated tetrahedra to chains, sheets, and finally complicated 3D frameworks.

The negative net electrical charge of the ion group must be compensated by cations to produce an electrically neutral compound. Constrained by the cosmic abundance of elements, these cations should be mostly Mg and Fe for silicates in space. The cations are dispersed between the individual tetrahedra or the tetrahedra arrays. Mineral structures that have been extensively discussed in the context of cosmic dust are nesosilicates (isolated tetrahedra, $[SiO_4]^{4-}$ anion), inosilicates (single chain, $[SiO_3]^{2-}$ anion), and phyllosilicates (sheets, $[Si_2O_5]^{2-}$ anion). In the case of inosilicates, the tetrahedra share two O atoms, whereas the tetrahedra in the continuous sheets of phyllosilicates share three O atoms.

The astrophysically interesting groups of olivine and pyroxene minerals belong to the silicate classes of nesosilicates and inosilicates, respectively. Olivines are characterized by isolated $[SiO_4]^{4-}$ tetrahedra that are linked by divalent cations. Pyroxenes are formed by single chains of such tetrahedra. According to their lattice symmetry, the olivines belong to the rhombic crystal system. In contrast to olivines, pyroxenes can occur in two different main crystallographic systems. The lattice can be of rhombic or monoclinic structure. An image of an olivine crystal is shown in **Figure 2**.

The general sum formula of olivines is $Mg_{2x}Fe_{2-2x}SiO_4$ with x between 1 and 0. The Fe and Mg cations can replace each other in the crystal structure. This means that olivines can be considered as solid solutions of Mg_2SiO_4 and Fe_2SiO_4. The two end members of these isomorphous crystalline compounds are forsterite (Mg_2SiO_4) and fayalite (Fe_2SiO_4). The atomic structure of olivine is best described as a hexagonal close-packed arrangement of O ions with octahedral sites occupied by Mg or Fe ions (see **Figure 3**).

Pyroxenes have the symbolic formula $Mg_xFe_{1-x}SiO_3$ with x between 1 and 0. The metal ions, which link the chains, are coordinated by six O atoms. The Fe-free and Mg-free end members of this group are enstatite and ferrosilite.

Another interesting group of crystalline silicates are hydrous silicates, mostly crystallizing in the form of layer-lattice silicates. In the case of phyllosilicates, layers of silicate tetrahedra are combined with OH layers. The crystal layers can be linked through interlayer cations, H bonds, interleaved hydroxides, or van der Waals forces. An example is the hydrous silicate talc with the chemical formula $Mg_3(OH)_2[Si_2O_5]_2$. In this case, brucite ($Mg(OH)_2$) layers are inserted between the silicate planes. Such silicates can only form in aqueous environments.

Figure 2

Image of an olivine crystal. The size of the crystal is about 1.2 cm × 0.7 cm × 0.5 cm.

Silica, or silicon dioxide (SiO_2), is a special case with no negative charges and no need for counter ions. Silica forms very complicated 3D networks. All O atoms of a given tetrahedron are shared with the neighboring tetrahedron. An example of this group of materials is the mineral quartz.

All the crystalline materials discussed so far have a periodic (long-range) order. Amorphous silicates are built of the same basic structural units as the crystalline silicates, the SiO_4 tetrahedra. However, they do not show periodic structures and are characterized by a 3D disordered network (see **Figure 4**). The incorporation of metal cations in the silicate network leads to a partial destruction of the O bridges and the formation of nonbridging O. In the produced hollow space, the cations are coordinated by bridging and nonbridging O atoms. However, small cations like

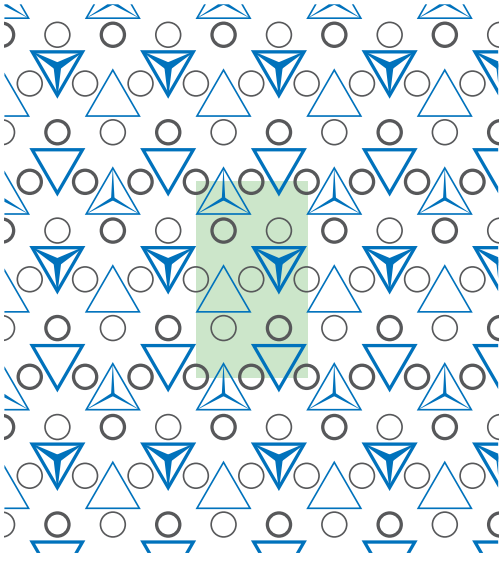

Figure 3

The crystalline structure of olivine represented by the packing of SiO_4 tetrahedra (*blue*) and metal cations (*gray circles*). The silicon atom at the center of the tetrahedron is not shown. The light green area indicates the extent of the elemental cell.

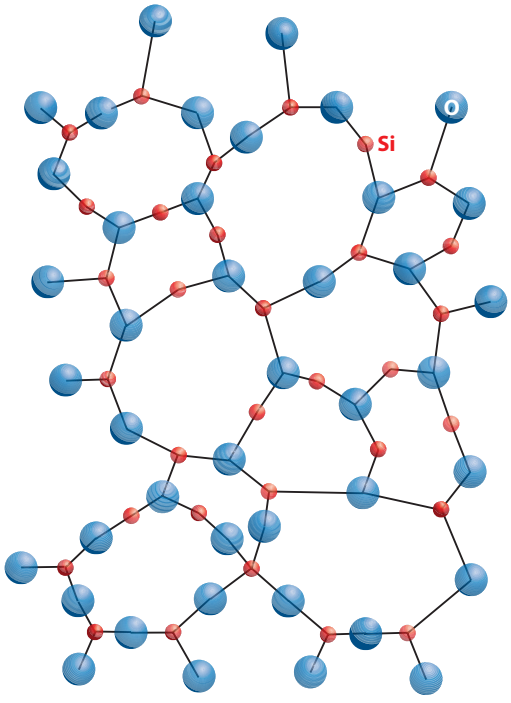

Figure 4

Schematic structure of amorphous SiO_2. Oxygen atoms are shown as blue spheres.

Mg^{2+} can act as network formers and can replace the Si atom in the SiO_4 groups. The amorphous structure can be represented by a mixture of different arrangements of SiO_4 tetrahedra in islands, small chains, rings, and sheets on small scales.

Phase transitions between amorphous and crystalline silicates lead to strong changes in a variety of physical properties, including the optical response function of the material. Here we should note that the terms olivines and pyroxenes are reserved for minerals with definite crystal structure and should not be used for amorphous materials.

2.2. Optical Properties

Amorphous silicates generally show two broad IR bands at about 10 and 18 μm, corresponding to Si–O stretching and O–Si–O bending vibrations, respectively. These silicate features can occur in emission, absorption, or self-absorption, depending on the optical depth of the medium. The large width of the bands results from a distribution of bond lengths and angles typical of amorphous silicates. The 18-μm band is additionally broadened due to the coupling of the bending mode to the metal-O stretching vibration located in this spectral region. The intrinsic ratio of the peak strengths of the 18- to 10-μm band varies typically between 0.3 and 0.7.

The position of the Si–O stretching vibration depends on the level of SiO_4 polymerization. As an example, the band is shifted from 9 μm for pure SiO_2 to 9.7 μm for $MgSiO_3$ to about 10.25 μm for $Mg_{2.4}SiO_{4.4}$ (Jäger et al. 2003a). The Mg/Fe ratio plays a major role in determining the absorptivity at near-IR and optical wavelengths (Ossenkopf, Henning & Mathis 1992). This is a critical feature for grain heating and transfer of radiation pressure in environments where the radiation field peaks in this wavelength range. In the case of a glass with pyroxene composition, Dorschner et al. (1995) demonstrated experimentally that the absorptivity increases strongly with Fe content.

In contrast to the amorphous silicates, crystalline pyroxenes and olivines produce a wealth of narrow bands from the mid-IR to the far-IR range due to metal-O vibrations (Koike, Shibai & Tsuchiyama 1993; Jäger et al. 1998). Generally, the spectrum can be divided into three main spectral regions. The bands between 1100 and 800 cm^{-1} (wavelength range between 9.0 and 12.5 μm) correspond to different asymmetric and symmetric stretching vibrations of the SiO_4 tetrahedra. The various features between 700 and 470 cm^{-1} (wavelength range between 14 and 22 μm) are caused by bending vibrations of the SiO_4 tetrahedra. The far-IR bands in the low-frequency region beyond 470 cm^{-1} can be attributed to translational motions of the metal cations within the O cage and complex translations involving metal and Si atoms.

Olivines show asymmetric stretch vibration bands in the 10- to 11.6-μm range and Si–O–Si and O–Si–O bending modes at 16, 20, and 23 μm. Metal-O translational vibrations occur in the range between 33 and 40 μm. Pyroxene spectra are usually somewhat more complex owing to the polymerization of the SiO_4 groups. Forsterite has strong bands at 10.0, 11.3, 16.3, 23.5, 27.5, and 33.5 μm, with a weaker, but characteristic band at 69.7 μm. Clinoenstatite displays strong bands at 9.4, 9.9, 10.6, 11.1, 11.6, 18.2, 19.3, and 21.5 μm with a forest of weaker and broader bands at longer wavelengths (Jäger et al. 1998).

In crystalline pyroxenes and olivines, the majority of the IR peaks are shifted to longer wavelengths with increasing Fe content. The observed shift is caused by an increase in bond lengths between the metal cations and the O atoms when Mg^{2+} is substituted by Fe^{2+}. The wavenumber shift is very closely correlated with the Fe content and allows us to derive the Mg/Fe ratio from IR spectroscopy (Jäger et al. 1998). An example is the 33.5-μm olivine band, which practically disappears in fayalite.

The far-IR continuum behavior of small amorphous silicate particles with olivine and pyroxene stoichiometry is often characterized by a power-law dependency of the absorption efficiency with wavelengths having an index close to −2 (e.g., Dorschner et al. 1995). This behavior is caused by the phonon spectrum of the material. Crystalline silicates show a similar wavelength dependency of the absorption efficiency reflecting the long-wavelength wing of Lorentz oscillators (e.g., Mennella et al. 1998).

The temperature of the silicate grains can play an important role in determining the position and shape of features and the long-wavelength continuum absorption. The general physical basis of these effects for cosmic dust analogs was summarized by Henning & Mutschke (1997). The vibrational bands of the silicates broaden and shift to longer wavelengths with increasing temperature. This behavior is especially pronounced for features at longer wavelengths (Koike et al. 2006). Crystalline forsterite possesses sharp and isolated far-IR bands at 49 and 69 μm. Their temperature dependency may even be used as a dust thermometer (e.g., Bowey et al. 2001, Koike et al. 2006). The absorption efficiencies of amorphous silicates at submillimeter/millimeter wavelengths decrease significantly with temperature, and the spectral slope of the absorptivity becomes steeper (e.g., Mennella et al. 1998 and Boudet et al. 2005, and references therein).

We expect that cosmic silicates form a system of small particles with an optical response function different from the bulk material. Particle size, shape, and internal structure play an important role in determining the position and shape of the silicate features (e.g., Min et al. 2006, 2008a; Voshchinnikov et al. 2006; Voshchinnikov & Henning 2008; Mutschke, Min & Tamanai 2009). In **Figure 5**, we provide examples for these shape effects. We note that larger grains no longer show strong IR features and that IR spectroscopy can only trace the population of submicron- to micron-sized grains.

In order to evaluate the magnitude of size and shape effects, the complex optical constants of the material (or the dielectric function) as a function of wavelengths have to be known. A compilation of these quantities for astronomically relevant materials can be found in the Heidelberg-Jena-St.

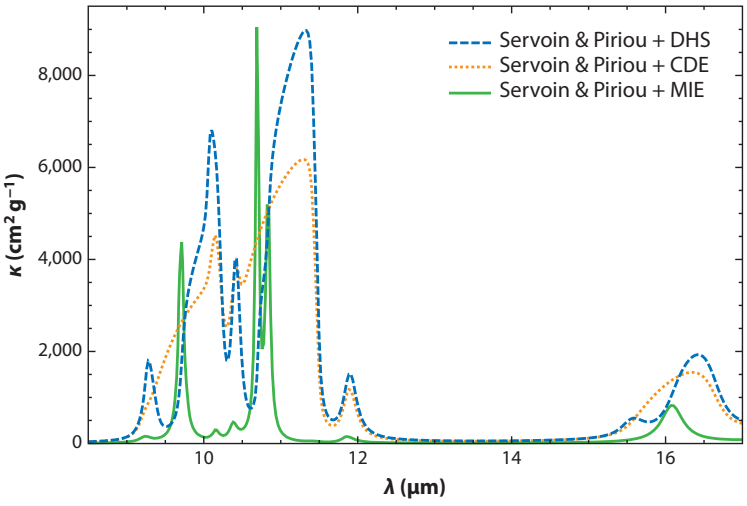

Figure 5

Mass absorption coefficients for small forsterite grains with different shape distributions. Abbreviations: DHS, distribution of hollow spheres; CDE, continuous distribution of ellipsoids; MIE, spherical particles. The optical constants for the calculations are taken from Servoin & Piriou (1973).

Petersburg database [described by Henning et al. (1999) and Jäger et al. (2003c); the database can be accessed via **http://www.mpia-hd.mpg.de/HJPDOC**]. Valuable data sets have been published by the Jena Laboratory Astrophysics Group in a whole series of papers, both for amorphous and crystalline silicates (e.g., Dorschner et al. 1995, Jäger et al. 1998, Fabian et al. 2001), as well as by various groups in Japan, especially for very clean crystals (e.g., Koike et al. 2003; Suto et al. 2002, 2006; Sogawa et al. 2006) and for hydrosilicates (Hofmeister & Bowey 2006; Glotch, Rossman & Aharonson 2007; Mutschke et al. 2008). For forsterite a frequently used set of optical constants has been published by Servoin & Piriou (1973). Data for α-quartz can be found in Spitzer & Kleinmann (1961) and Gervais & Piriou (1975).

Here we note that the optical data provided for crystals of the same composition may differ because of stacking faults, defects, and impurities (e.g., Murata et al. 2009). This may allow us to distinguish between spectra produced by pure crystals and annealed amorphous silicates, which may still contain stacking faults (Molster et al. 2002b).

Crystals often show different optical constants along the different crystal axes so that more than one set of optical constants has to be used and the absorption and scattering efficiencies have to be properly averaged for an ensemble of particles. We refer to Bohren & Huffman (1983) for an excellent textbook describing the fundamentals of scattering theory and the tools to calculate the absorption and scattering properties for small particles.

We also note that the shape of silicate emission features does not only depend on the absorption and scattering efficiencies, but also on the temperature of the grains via the Planck function. These dust temperatures can be computed with radiative transfer calculations if the external stellar or interstellar radiation fields and the geometry of the dust configurations are known. In addition, the optical constants must be available over a wavelength range relevant for the calculation of the energy balance.

2.3. Processing of Cosmic Silicates

During the life cycle of silicates, a variety of processes will modify the structure of this dust component. The annealing of freshly formed dust grains may already occur in the envelopes around AGB stars. Collisional grain destruction is certainly a limiting factor for the supernova

dust yield. In the diffuse ISM, a multitude of processes can be expected to operate, including sputtering and thermal erosion, collisional fragmentation, and chemical and structural processing by irradiation. In protoplanetary disks, sublimation and recondensation, thermal annealing, and irradiation by stellar wind ions have to be considered. Phase conversions from the amorphous into the crystalline state and vice versa are essential for the understanding of silicate evolution in space. Here, we discuss some experimental results with relevance for the evolution of cosmic silicates.

2.3.1. Thermal annealing. The conversion from the amorphous into the crystalline state can be caused by thermal annealing at sufficiently high temperatures. In general, crystallization is a complex process, including nucleation and crystal growth. IR spectroscopy has often been used for monitoring the progress of thermal annealing (e.g., Hallenbeck, Nuth & Daukantas 1998; Brucato et al. 1999; Fabian et al. 2000; Jäger et al. 2003a), although alternative techniques such as synchrotron techniques and high-resolution electron microscopy are equally important (e.g., Thompson 2008). A qualitative description of the timescale of crystallization is provided by the equation $\tau^{-1} = \nu_0 \exp(-E_a/kT)$, where E_a is the activation energy, T is the dust temperature, and k is the Boltzmann constant. The quantity ν_0 represents a constant proportional to the mean vibrational frequency of the silicate lattice ($\nu_0 = 2 \times 10^{13}$ s^{-1}). This equation immediately demonstrates the strong temperature dependency of the annealing process. As soon as the "right" annealing temperature is reached, the transformation of amorphous into crystalline silicates is a fast process.

In the annealing experiments of amorphous silicate and Mg-Fe silicate smoke, Hallenbeck, Nuth & Daukantas (1998) found relatively high E_a/k values of 45,500 K. Further experiments on more homogeneous materials provide lower values of activation energies in the range between 38,500 and 39,100 K (Fabian et al. 2000). Because the crystallization process is strongly related to the diffusion of metal and O atoms, the activation energy depends on the viscosity behavior during annealing. The incorporation of nonassociated OH^- or Fe^{2+} ions decreases the viscosity (internal resistance of the system to flow) at the annealing temperatures and leads to much lower activation energies. As a result, the annealing temperature and the annealing time can be considerably reduced by the presence of OH in the silicate network (Jäger et al. 2003a). The incorporation of OH groups during the condensation process of circumstellar silicates is a likely process, because H_2O certainly participates in the formation of olivine- and pyroxene-type silicates (Gail & Sedlmayr 1998).

Crystallization experiments on amorphous Mg silicates revealed that the IR features of the produced enstatite are different from those of fine powdered single crystals (Murata et al. 2009). Murata et al. related this finding to abundant stacking faults and concluded that these bands fit circumstellar silicate profiles better. However, we note again that particle shape effects play a major role in determining the profiles and have not been investigated in these experiments.

The direct formation of crystalline silicates from the vapor phase has also been discussed (e.g., Nagahara et al. 2010). In such an experiment, Kimura et al. (2008a) were able to produce crystalline silicates due to the production of a large amount of exothermic energy by the oxidation of Mg.

A more exotic crystallization process was studied by Kimura et al. (2008b). They induced crystallization to forsterite by electron-beam irradiation of amorphous Mg-bearing silicates. The crystallization process was much accelerated by the presence of CH_4 adsorbed to the surface and incorporated into the interior of the grains. This process must still be demonstrated as being of general importance for cosmic silicates and efficient enough to convert amorphous into crystalline silicates under astronomically relevant conditions.

2.3.2. Irradiation of silicates. Irradiation of silicates with energetic ions has attracted a lot of attention in the context of silicate amorphization. Direct atom displacements through nuclear

interactions and ionization are key processes that can lead to a modification of the silicate structure (Leroux 2009).

Experimental studies have investigated amorphization of silicates by irradiation with low-energy (kiloelectronvolt) ions (mainly protons, helium and argon ions) with fluences typical of what can be expected in high-velocity supernova shock fronts (e.g., Demyk et al. 2001, 2004; Jäger et al. 2003b; Brucato et al. 2004). An efficient amorphization by light ions can only be observed for low energies (below 50 keV). According to computational and experimental results, 50-keV helium ions can amorphize crystalline enstatite grains up to a penetration depth of 360 nm at a fluence of 9×10^{16} ions cm^{-2}. This penetration depth is larger than the typical 0.1-μm size of interstellar grains. Wang, Miller & Ewing (1993) observed amorphization through 1.5-MeV Kr^+ irradiation with a fluence of 5×10^{14} ions cm^{-2}. In these experiments, elastic atomic interactions are the main reason for the observed phase transition from the crystalline to the amorphous state.

In the case of irradiation with high-energy (≥MeV) ions, frequent ionization events occur along the particle trajectories, corresponding to a high-energy deposition rate. The overlap of these "irradiation tracks" can finally lead to complete amorphization of the material. In general, lower fluence values are required for amorphization. Bringa et al. (2007) demonstrated the amorphization of single-crystal forsterite when irradiated by 10-MeV Xe ions at a fluence of only 3×10^{13} ions cm^{-2}.

In experiments with very low-energy ions, the chemical composition of silicates can change as a result of selective sputtering (Leroux 2009). An example is the experiment by Demyk et al. (2001) with low-energy He^+ ions (4–10 keV) and a fluence of 1×10^{18} ions cm^{-2}. Here amorphization of forsterite was accompanied by a chemical alteration from olivine to pyroxene stoichiometry. A depletion of MgO has been found due to the selective sputtering of Mg and O. In addition to amorphization and chemical alteration, changes in the morphology of the grains can also be observed. The formation of pores and/or He bubbles and the erosion of grain edges has been seen in a number of experiments (e.g., Jäger et al. 2003b).

Rietmeijer (2009) reported direct evidence for the irradiation-induced amorphization of crystalline olivine to glass with pyroxene composition in chondritic interplanetary dust grains. This finding demonstrates the importance of irradiation-induced amorphization processes for cosmic silicates.

3. SILICATES AROUND EVOLVED STARS

Asymptotic giant branch (AGB) stars are among the most important sources of freshly formed dust (e.g., Gail et al. 2009). A crucial aspect for dust formation in the circumstellar environment of these low- and intermediate-mass stars is the relative abundance of C and O. In M-type stars, the C/O ratio is smaller than 1; all the carbon should be bound in the stable CO molecule and the formation of O-rich dust can be expected. The investigation of the chemical equilibrium composition of the dust-gas mixture in the winds of evolved O-rich stars predicts the formation of Fe, forsterite (Mg_2SiO_4), and enstatite ($MgSiO_3$) (Gail 2010). The Fe content should be very low for $T > 700$ K, and the occurrence of pure forsterite and enstatite grains can be expected. At much lower temperature ($T \leq 600$ K) the Fe content in a chemical equilibrium mixture rapidly increases with decreasing temperature, but equilibration is certainly prevented. The grains that form at the lower temperatures should be in the amorphous state and should contain some Fe. For a more comprehensive treatment of the formation and evolution of minerals in AGB star winds, we refer to the review by Gail (2010), which also includes a discussion of the relevant experimental literature.

Broad and structureless bands at 10 and 18 μm have been frequently observed in the spectra of evolved stars, including AGB stars, post-AGB stars, planetary nebulae, and luminous blue variables.

Figure 6

Comparison of the continuum-subtracted spectrum of the object AFGL 4106 with the mass absorption coefficient of forsterite (*purple line*) and enstatite grains (*red line*) multiplied by a Planck curve of 100 K and normalized to 1. AFGL 4106 is a double-line spectroscopic binary; the warmer component is likely a post-Red-Supergiant. After Jäger et al. (1998).

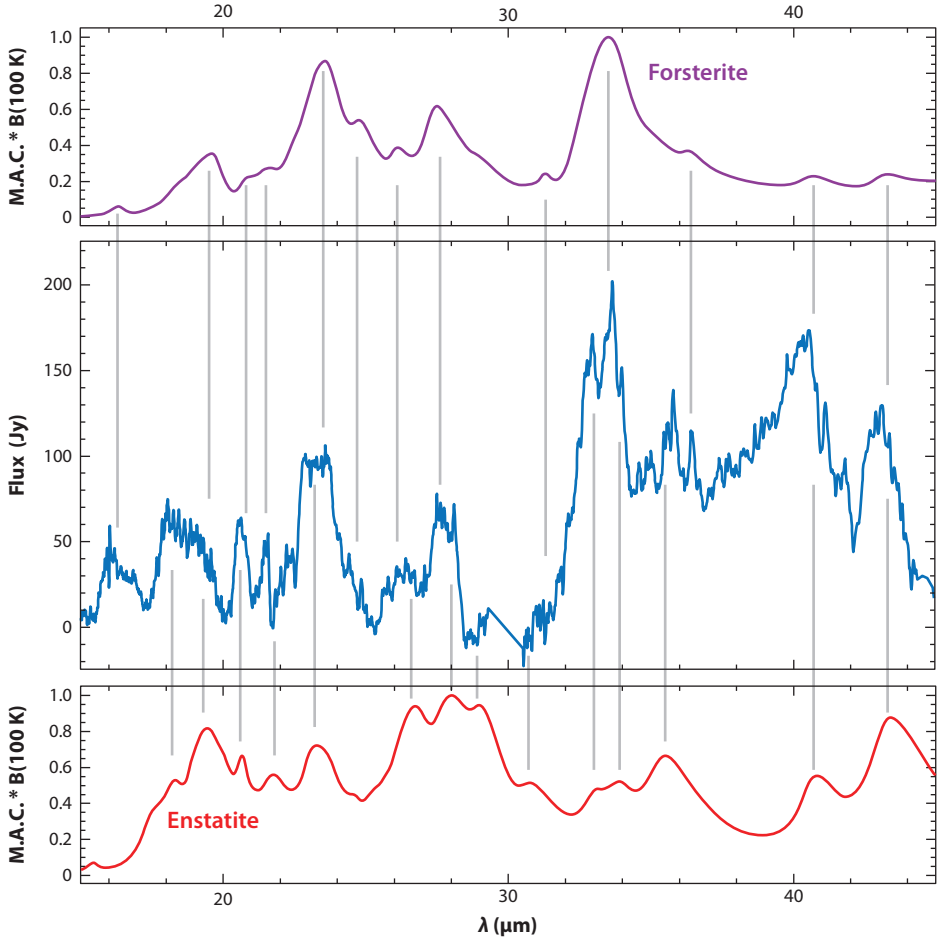

They were generally attributed to amorphous silicates and could be well fitted with laboratory data for amorphous silicates with olivine-type stoichiometry (e.g., Dorschner et al. 1995). The observed "amorphous" bands show a considerable variety of band positions and shapes, indicating different grain sizes, morphology, and chemical composition.

The *Infrared Space Observatory* (ISO) with its two spectrometers, covering a wavelength range between 2 and 200 μm, led to breakthroughs in the characterization of AGB star spectra. Finally, the fingerprint spectra of cold crystalline sillicates could be detected (Waters et al. 1996). A forest of narrow features in the wavelength range between 20 and 70 μm could be attributed to olivines and pyroxenes (Jäger et al. 1998; Molster, Waters & Tielens 2002a). The analysis of the band positions, especially the 69-μm olivine band and the 40.5-μm pyroxene band, clearly indicates that the crystalline silicates are Fe-poor and Mg-rich in composition (see **Figure 6**). The relative abundance of crystalline silicates is in general quite modest (10%–15%), but sources with disk-like geometry often show very strong bands owing to crystalline silicates (Molster, Waters & Tielens 2002a). The crystalline silicates are in general colder than the amorphous silicates, indicating that amorphous silicates contain some Fe, leading to higher near-IR absorptivity (Molster et al. 2002b). This "dirtiness" of the amorphous silicates (Jones & Merrill 1976) could be produced by Fe within the

silicates (Dorschner et al. 1995) or admixtures of metallic Fe to the silicates (Ossenkopf, Henning & Mathis 1992). The finding that crystalline silicates are Fe-poor and that the amorphous silicates should contain some Fe is very much in agreement with the expectations from the condensation sequence, discussed at the beginning of this section. Indications for crystalline silicates have also been seen in the spectra of post-AGB stars, supergiants, planetary nebulae, and luminous blue variables.

We note that silicate features, including evidence for crystalline silicates, have also been found in C-rich objects, including planetary nebulae (Waters et al. 1998a) and the prominent O-rich dust disk around the central star of the Red Rectangle (Waters et al. 1998b). This silicate dust was likely produced in previous O-rich mass-loss episodes. Disk structures may play an important role in storing this material (e.g., Yamamura et al. 2000).

With the much increased sensitivity of the *Spitzer Infrared Telescope* (*Spitzer*) compared to ISO, dust spectroscopy of evolved stars could readily be extended to sources in the Large Magellanic Cloud (LMC). First evidence for the presence of extragalactic crystalline silicates was obtained in an ISO spectrum of the luminous blue variable R71 (Voors et al. 1999). *Spitzer* spectroscopy demonstrated the widespread appearance of silicate features in the spectra of evolved stars in the LMC, including evidence for crystalline silicates (e.g., Kastner et al. 2006; Sloan et al. 2006, 2008; Zijlstra et al. 2006).

The analysis of silicate stardust grains in primitive meteorites provides a new information channel on the chemical composition, structure, and formation history of circumstellar silicates. Sensitive and small-scale mapping of the Si and O isotopes in stardust silicates has only become possible with the recent advancement in ion microprobe technology. The NanoSIMS instruments allowed the in situ identification of submicron-sized silicate stardust grains in carbonaceous chondrites (Mostefaoui & Hoppe 2004, Nguyen et al. 2007). These presolar grains have olivine, pyroxene, and glass-like compositions. In fact, most of the presolar silicates found in carbonaceous chondrites seem to originate in AGB stars (Vollmer, Hoppe & Brenke 2008). A microstructural analysis of presolar grains with isotopic composition, implying an AGB star origin, has been performed by Vollmer et al. (2009). They found three amorphous Mg-rich silicate grains with a variable but more pyroxene-like composition. Three grains are Fe-bearing glasses. In addition, two olivine grains were found, one with a relatively high Fe content. We can expect to see more such studies in the future, which will allow researchers to make a connection between the results from IR spectroscopy and the laboratory analysis of stardust particles.

4. SUPERNOVA DUST

Dust production has been discussed for a variety of supernova types, although most of the attention has been paid to dust formation by type II supernovae. Based on classical nucleation theory, which has its own limitations, Kozasa, Hasegawa & Nomoto (1989, 1991) investigated the formation sequence of dust in the ejecta of SN 1987A and concluded that the composition of the dust grains is mostly defined by the elemental composition of the gas. Although type II supernovae may efficiently produce dust, the reverse shock may actually destroy most or all of the newly formed dust particles (Nozawa et al. 2007). Although the overall amount of dust produced in supernovae is still under debate, it is very likely to be small compared to other dust sources.

All kinds of O-rich dust have been considered as potential condensates, including SiO_2 and silicate particles. Evidence of silicate grains has been found in the *Spitzer* spectra of the ejecta of the young SN remnant 1E0102-7219 in the Small Magellanic Cloud (SMC) (Rho et al. 2009). The first direct spectroscopic evidence for the formation of silicate dust in the ejecta of a type II supernova has been found by IR observations of the supernova 2004ET (Kotak et al. 2009).

Some dust grains with isotopic anomalies typical of *r*-process composition associated with type II supernovae have been found in primitive meteorites (Clayton & Nittler 2004). Recently, Messenger, Keller & Lauretta (2005) identified a submicrometer-sized crystalline silicate grain in an anhydrous interplanetary dust particle with an isotopic composition typical of formation from a type II supernova. The supernova grain was identified as a polycrystalline aggregate of Fe-bearing forsterite.

5. SILICATES IN PROTOPLANETARY DISKS AND DEBRIS SYSTEMS

In protoplanetary disks, a large variety of physical processes modify the properties of interstellar grains entering these systems from their parental molecular clouds: thermal annealing and shock heating, flash heating, irradiation, sublimation and recondensation, grain growth, radial and vertical transport, and turbulent mixing processes. It would go far beyond this review on cosmic silicates to provide a comprehensive discussion of all these processes. For recent reviews on dust evolution in protoplanetary disks, we refer to Henning & Meeus (2010) and Watson (2010) and the book by Apai & Lauretta (2010).

In protoplanetary disks we expect the presence of amorphous interstellar silicates with nonequilibrium compositions in the outer disk regions, annealed amorphous grains in the more inner regions, and crystalline dust with chemical equilibrium composition in the innermost parts of the disks (Gail 2004, 2010; see **Figure 7**). The most abundant dust components in these inner regions should be forsterite and enstatite. In addition, the presence of quartz (SiO_2) can be expected if the Si/Mg abundance ratio is sufficiently high. Ca- and Al-containing silicates can be present; they are stable in some parts of the pressure-temperature parameter space in protoplanetary disks. An example for such silicates is the monoclinic pyroxene material diopside ($MgCaSi_2O_6$).

IR spectroscopy provided an enormous amount of data on the composition of dust in protoplanetary disks. Earlier studies showed that T Tauri disks often exhibit 10-μm silicate features in emission (Cohen & Witteborn 1985; Gürtler et al. 1998; Natta, Meyer & Beckwith 2000). These features imply the presence of a superheated optically thin dust layer on top of the optically thick disk interior. It is only the IR emission of the population of small grains in this layer that provides information on the nature of dust in protoplanetary disks. In the case of efficient vertical mixing, the entire small dust population is traced by IR spectroscopy. Radial and vertical mixing of material can be driven by turbulent motions in protoplanetary disks. In addition, disk winds may play an important role in the radial transport of dust grains above the disk atmospheres.

In view of the radial temperature gradient in disks, measurements at shorter IR wavelengths characterize the inner disk composition, whereas longer wavelength data contain information on the outer disk. In comparing spectra from disks around brown dwarfs, T Tauri stars, and Herbig Ae/Be stars, one has to keep in mind that the radial location of the 10-μm versus 30-μm emission regions is different for different (sub)stellar heating sources. In other words, the same silicate feature may trace different radial regions of a disk. Kessler-Silacci et al. (2007) calculated that the 10-μm silicate feature probes radii between 0.5 and 50 AU in disks around Herbig Ae/Be stars, but only radii between 0.001 and 0.1 AU in brown dwarf disks.

The 10-μm silicate feature has frequently been used to trace grain growth from submicron sizes to grain sizes of a few microns (e.g., Henning & Meeus 2010 and references therein). As submicron-sized grains grow in size above a micron, their 10-μm feature becomes broader and flatter and finally disappears compared to the triangular shaped feature of the smaller grain population. The observed relationship between profile shape and strength of the feature can be well represented by changing the characteristic grain size over the range from 0.1 to 4 μm (van Boekel et al. 2003, Kessler-Silacci et al. 2006, Meeus et al. 2009). The frequently observed presence of grains of several

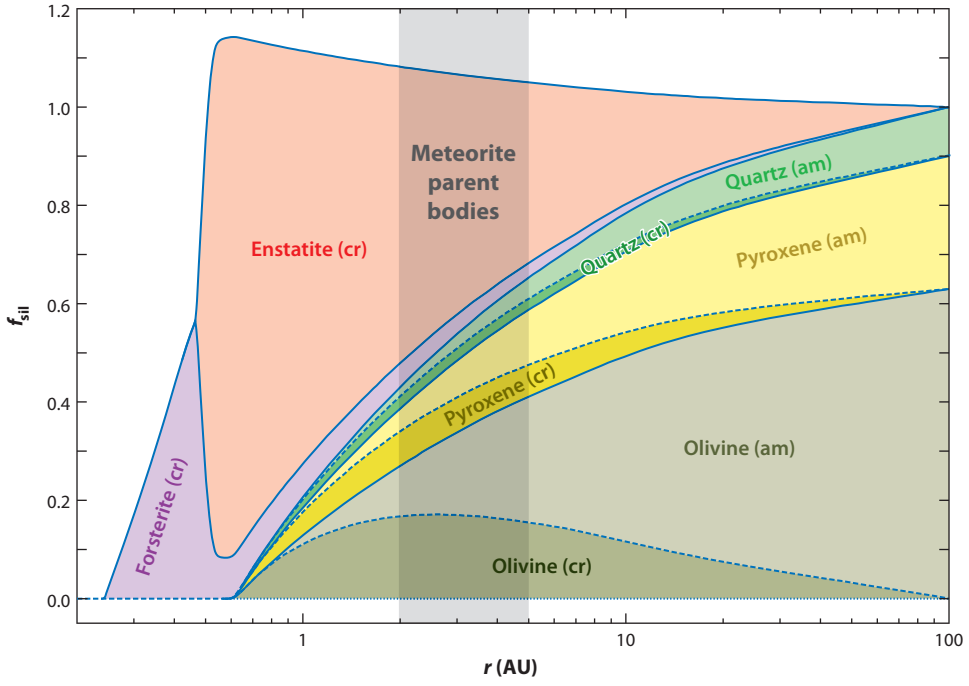

Figure 7

Cumulative representation of the radial distribution of silicon condensed in the various silicate dust components (interstellar and equilibrium dust). The total Si abundance is normalized to the interstellar abundance. An enhancement of the Si abundance in the region of evaporation is due to diffusive mixing. Pyroxene (am) and olivine (am) stand for amorphous interstellar grains with the chemical composition of pyroxene and olivine, respectively. The equilibrium dust components are always forsterite and enstatite (crystalline structure). The region where the parent bodies of meteorites in the Solar System form is indicated. For the calculations, a stationary disk model with an accretion rate of 10^{-7} M_{sun} $year^{-1}$ and a central star of 1 M_{sun} has been used. After Gail (2004).

microns in size in disk atmospheres argues for efficient replenishment of this grain component by vertically upward transport because these grains would rapidly settle in laminar disks. In fact, Sicilia-Aguilar et al. (2007) and Pascucci et al. (2009) found that objects with higher accretion rates have larger dust grains, indicating that turbulence supports larger grains against settling. Spectroscopy with ISO provided the first convincing evidence for the presence of crystalline silicates in the disk spectra of relatively bright Herbig Ae/Be stars (Bouwman et al. 2001, Meeus et al. 2001), with HD 100546 (Malfait et al. 1998) and HD 163296 (van den Ancker et al. 2000) being prominent examples. Silicates in the diffuse ISM and molecular clouds are predominantly in the amorphous state. The detection of crystalline silicates both in the inner warm parts of the disks and the colder outer regions implies that thermal annealing of dust, dust equilibration through sublimation and condensation processes, radial mixing, and shock heating certainly all contribute to the structure of protoplanetary dust. Most of the features in the two sources can be identified with forsterite grains. The amazingly perfect match of the "crystalline" features of HD 100546 with those detected in the ISO spectrum of comet Hale-Bopp (Crovisier et al. 1997) established an interesting link between protoplanetary dust and cometary material in our Solar System. The presence of crystalline silicates in comets was a quite unexpected finding because these objects were formed in the cold outer part of the Solar System, too cold for crystal formation.

They actually are thought to contain the most pristine material in the Solar System. Similar to cold crystals in protoplanetary disks, they must have formed through condensation and/or annealing processes together with transport processes, leading to an enhancement of the outer Solar System with crystalline silicates. We note that cometary silicate spectra show some diversity with clear differences between Jupiter-family comet dust and dust in Oort-family comets (Kelley & Wooden 2009). Interestingly, the analysis of particles, returned by the *Stardust* mission from comet 81P/Wild 2, showed in the majority of cases the presence of olivine (Zolensky et al. 2006). The typical sizes range from submicrometer to over 10 μm with a wide compositional range in Mg/(Mg+Fe) ratios.

Here, we note that HD 100456 is the only source among the observed Herbig Ae/Be stars where the 69-μm olivine band could be detected through ISO observations, which then allowed a clear determination of the Fe content and provided direct evidence for Fe-poor forsterite grains. However, also the shorter wavelength bands, especially in high S/N *Spitzer* spectra, point to a low Fe content in the crystalline silicates and can be well fitted by enstatite and forsterite (Juhász et al. 2010, Watson et al. 2009). In HD 100456 the abundance of forsterite increases with disk radius (Bouwman et al. 2003), which is not expected in the present generation of one-zone disk dust chemistry models (Bockelée-Morvan et al. 2002, Wehrstedt & Gail 2002, Gail 2004).

Bouwman et al. (2003) speculated about the possibility of a local production of small forsterite grains as the result of a collisional destruction process of a larger parent body as an explanation for the strong crystal bands in HD 100456. A very similar spectrum with a very large crystallinity fraction has meanwhile been observed with *Spitzer* for the M-type star RECX5 (age about 8 Myr) (Bouwman et al. 2010; see **Figure 8**). Both objects share similar disk structures and composition,

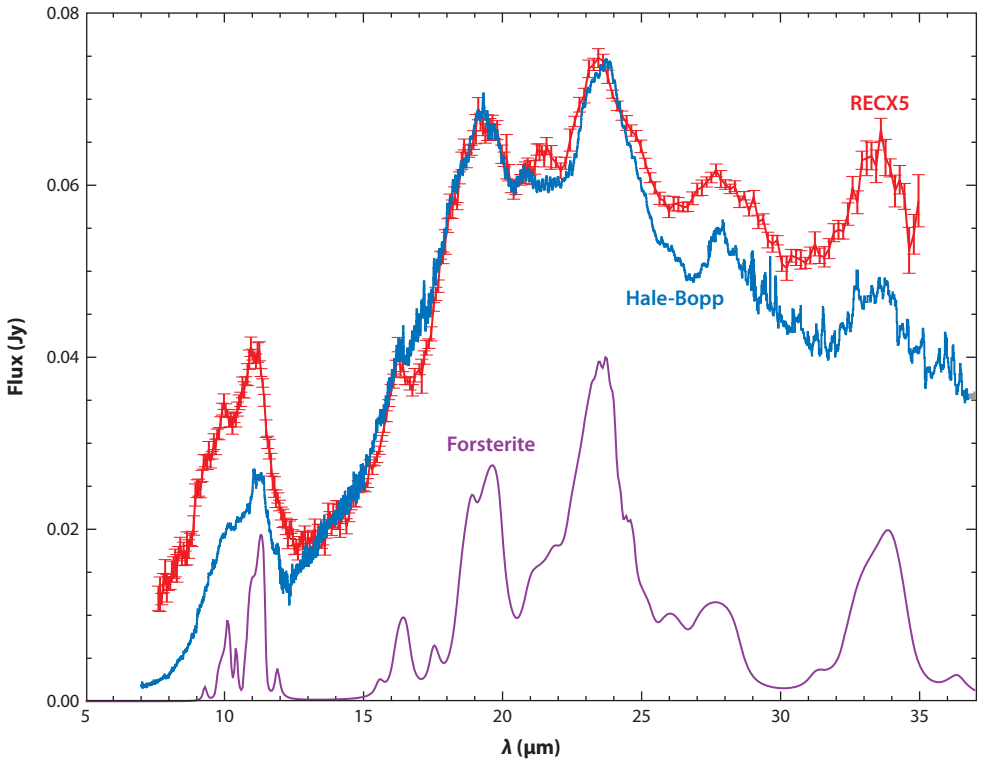

Figure 8

Comparison of the spectrum of the disk around the M-type star RECX5 (*red line*) and the scaled emission of the comet Hale-Bopp (*blue line*) (Crovisier et al. 1997). The purple lower line is an emission spectrum for a distribution of hollow forsterite spheres (compact equivalent radius of 0.1 μm) at 200 K. After Bouwman et al. (2010).

despite their very different spectral types. The spectral energy distributions indicate that the inner disk regions (<30 AU from the star) are relatively devoid of dust and that the outer disk is strongly flared.

In addition to silicates, SiO_2 grains have been detected in protoplanetary disks, both in the amorphous and crystalline states (Bouwman et al. 2001, van Boekel et al. 2005, Sargent et al. 2009, Juhász et al. 2010). The transparency of the material and the "warm temperature" emission favor a situation where the SiO_2 particles are in thermal contact with other grains, indicating the result of a partial annealing process. This is further supported by a correlation between the abundance of forsterite and silica, which has been found by van Boekel et al. (2005). Solid observational evidence for the presence of diopside in disks is not available.

Meanwhile, *Spitzer* spectroscopy provided an enormous amount of IR spectra of disk sources, ranging from very high S/N data of disks around Herbig Ae stars (Juhász et al. 2010) to faint brown dwarf disks (Apai et al. 2005). Crystalline silicates have been found in all kinds of protoplanetary disk environments, including Herbig Ae/Be stars (Juhász et al. 2010), T Tauri disks (Kessler-Silacci et al. 2006, Sicilia-Aguilar et al. 2007, Bouwman et al. 2008, Meeus et al. 2009, Olofsson et al. 2009, Watson et al. 2009; see **Figure 9**), and disks around brown dwarfs (Apai et al. 2005,

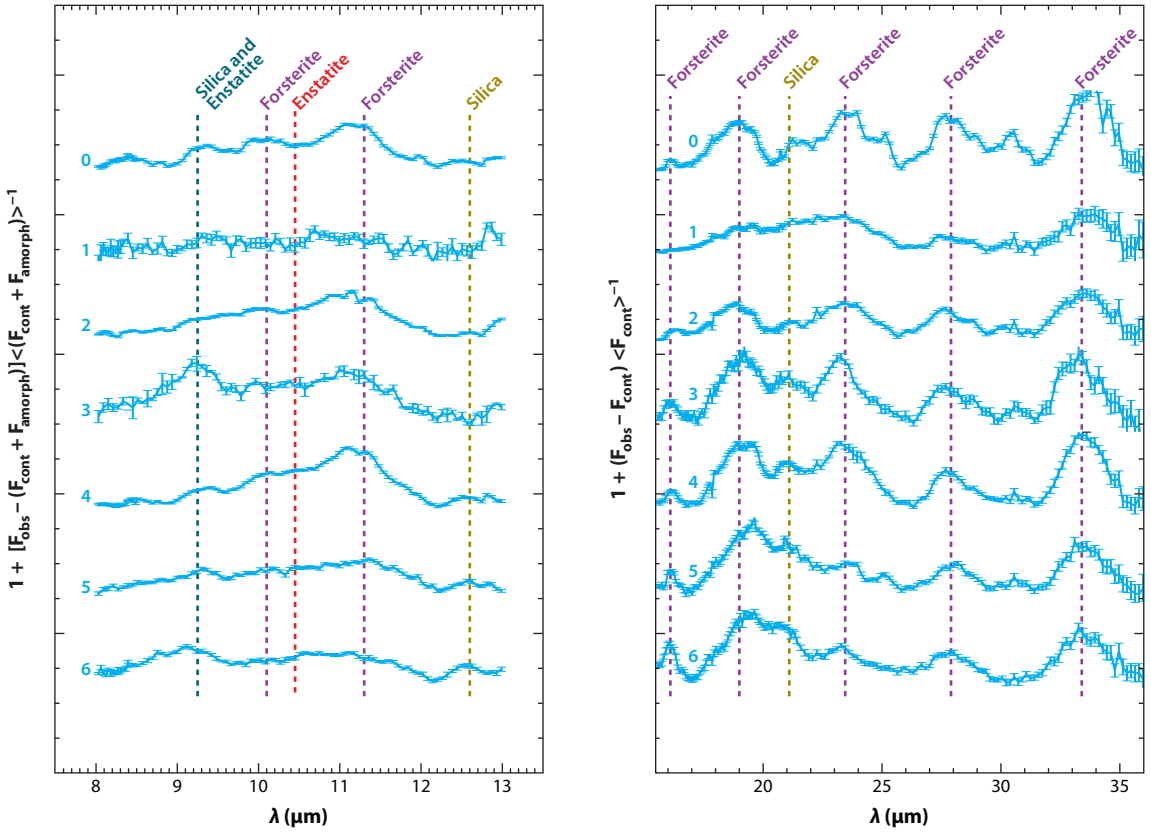

Figure 9

The emission bands of crystalline silicates (*light blue lines*) as observed with *Spitzer* in the spectra of seven T Tauri stars. The spectra have been normalized to a dust model fit, thereby removing the amorphous silicate—and, if present, the polycyclic aromatic hydrocarbon features—and enhancing the crystalline features. After Bouwman et al. (2008).

Merín et al. 2007, Pascucci et al. 2009). The occurrence of crystalline silicates in disks is a frequent phenomenon and not a rare situation. For the analysis of disk spectra in terms of grain size, crystallinity fraction, and chemical composition, different spectral fitting procedures have been used and care must be taken if values from different studies are compared (Juhász et al. 2009). In addition, models that contain small fractional abundances of rare species to fit spectra with low signal-to-noise ratios may lead to spurious results.

The mass fraction of small silicate particles in crystalline silicates typically ranges between a few percent and 40% with individual variations between inner and outer disks. Mid-IR interferometry studies with the VLTI of the very inner disks around three Herbig Ae stars and TW Hydrae show that in these regions the crystal mass fraction can be very high and decreases with distance from the star (van Boekel et al. 2004, Ratzka et al. 2007; see **Figure 10**). This is in agreement with the expectation of thermal annealing and/or crystal formation in gas phase condensation processes. In addition, van Boekel et al. (2004) found that the silicate crystals in the inner disk are predominantly of forsterite composition, as expected for an equilibrium situation in this region.

No obvious very strong correlation between crystallinity and stellar/disk parameters or age of the systems has been found. This suggests the importance of other processes such as irradiation or planet formation events. In fact, Glauser et al. (2009) demonstrated an anticorrelation between X-ray activity and crystalline mass fraction, implying amorphization of dust in the disk atmospheres. This effect could also erase other relations between crystallinity and disk/star parameters.

Studies of disk spectra from T Tauri stars (e.g. Bouwman et al. 2008, Meeus et al. 2009) and Herbig Ae stars (Juhász et al. 2010) indicate a change in the relative abundance of crystalline silicates of different composition with radial distance from the star: More enstatite relative to forsterite is observed in the inner warm disk population, whereas forsterite dominates in the colder outer regions (see **Figure 9**). The *Spitzer* spectra of the T Tauri stars in the 10-μm range typically trace inner disk regions around 1 AU, whereas the long-wavelength part of the spectra is produced in disk regions between 5 to 15 AU. The finding of forsterite as the dominant component in the outer disks is in contrast to the predictions of stationary disk models, including sublimation and condensation as well as radial mixing (e.g., Gail 2004), and may be an argument for more localized nonequilibrium crystal formation processes such as shocks as proposed by Harker & Desch (2002). Other explanations for this discrepancy include more complicated disk models, especially in the early phase of disk evolution, or nonequilibrium chemistry conditions for the outer disk, depending on initial grain composition and subsequent kinetic evolution. In addition, episodic heating events may play an important role in crystal formation. Ábrahám et al. (2009) reported such an episodic crystal formation process via annealing of material in the surface layer during an eruption of the young Sun-like star EX Lupi. This observation is the first direct observational evidence for the in situ formation of crystals in protoplanetary disks. In **Figure 11**, we compare the pre-outburst and the outburst spectra of EX Lupi with profiles of amorphous and crystalline grains, including an ISM silicate profile and silicate emission profiles from comets.

We note that the silicates in the disks around cool stars and brown dwarfs show weaker 10-μm emission features compared with disks around more massive stars, originating from more processed silicate grains (e.g., Sicilia-Aguilar et al. 2007, Pascucci et al. 2009). This could be explained either by the fact that the silicate emission in disks around brown dwarfs/cool stars comes

Figure 10

Infrared spectra of the inner (1–2 AU) and outer (2–20 AU) disk regions of three Herbig Ae stars. The regions that dominate the inner- and outer-disk spectra are indicated in the schematic disk representation at the top of the image (not to scale). Also shown are the best-fit model spectra for the inner- and outer-disk regions (*gray lines*). After van Boekel et al. (2004).

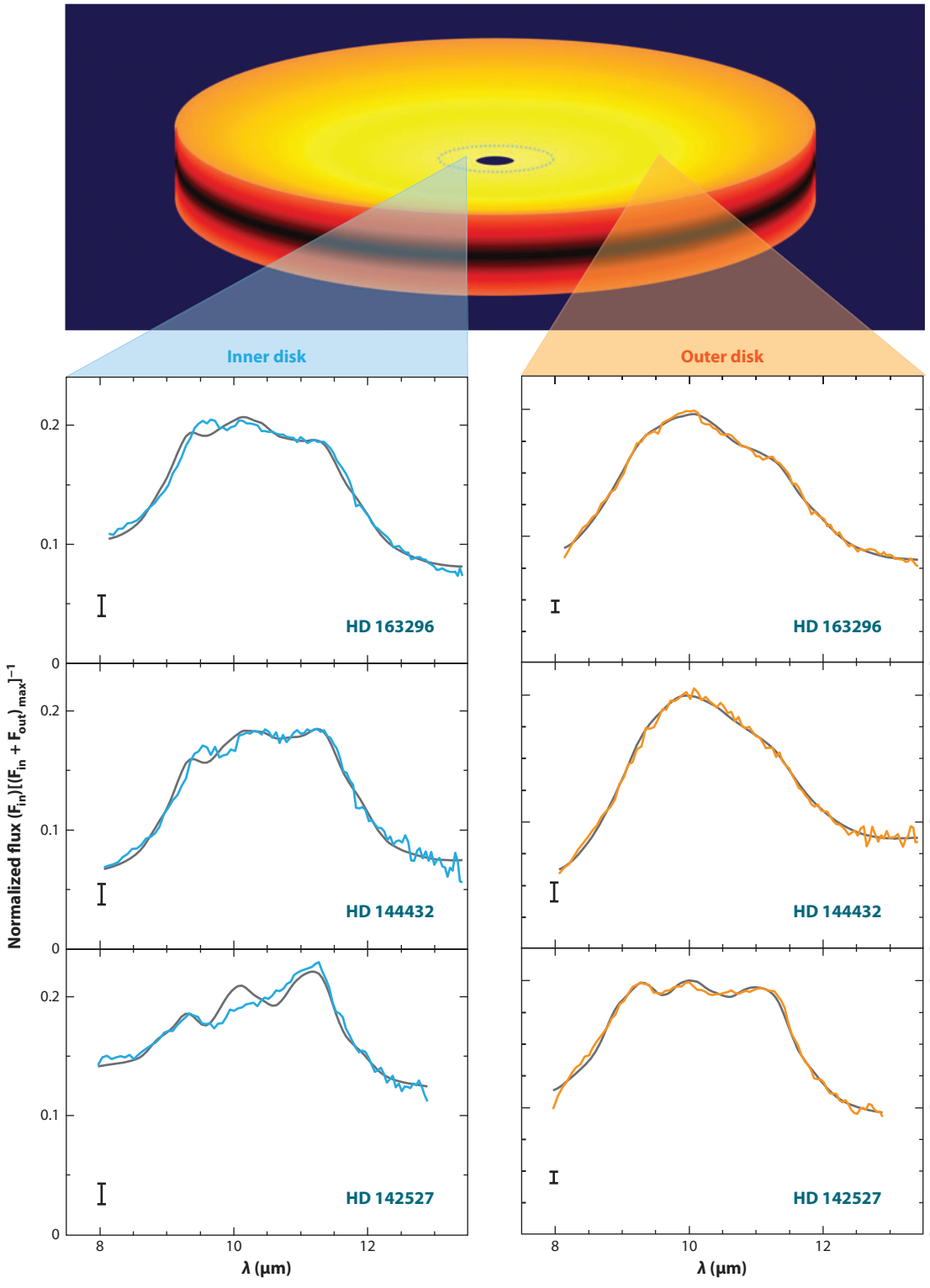

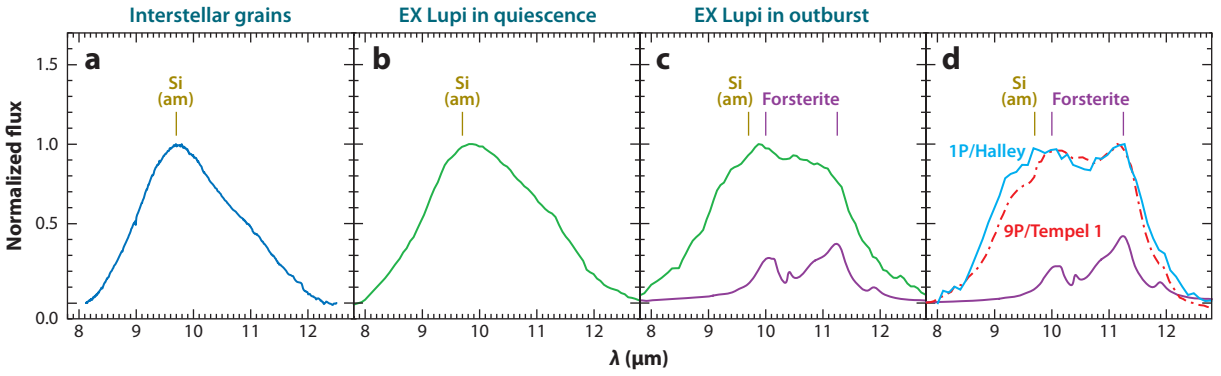

Figure 11

Formation of silicate crystals during the outburst of the young Sun-like star EX Lupi. Shown are the silicate emission features in the wavelength range between 8 and 12 μm. (*a*) Spectrum of interstellar silicate grains measured in the direction to the Galactic center for comparison. After Kemper et al. (2004). The characteristic triangular shape can be attributed to amorphous silicate grains. The vertical line at 9.7 μm (repeated in all panels) corresponds to the peak wavelength of an amorphous silicate profile as measured in the laboratory. After Dorschner et al. (1995). (*b*) *Spitzer* spectrum of EX Lupi in quiescent phase (March 18, 2005). The spectrum closely resembles the profile of amorphous silicates. (*c*) *Spitzer* spectrum of EX Lupi in the middle of the recent outburst (April 21, 2008). Peaks and shoulders due to crystalline silicates can be identified. Peak wavelengths of forsterite at 10.0 and 11.2 μm, as measured in laboratory experiments (Jäger et al. 1998, Koike et al. 2003), are indicated. (*d*) Solid light blue line: Ground-based spectrum of Comet 1P/Halley (Hanner, Lynch & Russell 1994); dash-dotted red line: *Spitzer* spectrum of the ejecta from Comet 9P/Tempel 1 during the Deep Impact Experiment from the *Spitzer* archive (see also Lisse et al. 2006). After a linear continuum removal, the spectra were normalized to their peak values. The cometary spectra show the same crystalline features as in the outburst spectrum of EX Lupi. The lower purple curves in panels *c* and *d* display the emissivity curve of pure forsterite (Koike et al. 2003), assuming a representative silicate grain temperature of 1,250 K and 300 K, respectively. After Ábráham et al. (2009).

from more inner and, therefore, more evolved disk regions or by a spectral-type-dependent dust composition.

Silicate features are usually not detected in IR spectra of debris disks (e.g. Carpenter et al. 2009). An explanation could be that the lifetime of smaller particles is so short that they can only be observed after certain production events. The general IR excess emission from debris disks simply comes from larger grains, which display no IR features, or/and is associated with colder dust. A prominent exception to the featureless spectra is β Pictoris, where evidence for amorphous and crystalline silicates could be found (Knacke et al. 1993, Chen et al. 2007). Another interesting source is the 2-Gyr-old star HD 69830, which is associated with Neptune-mass planets. The spectrum of this object shows prominent features due to warm crystalline grains (Beichman et al. 2005). Beichman et al. pointed out that the collisional and Poynting-Robertson drag times are shorter than 100 years. They concluded that the small silicate grains are created by collisional grinding of material in an asteroid belt or a single super comet. A few more such examples of warm debris disks with silicate features can be found in Moór et al. (2009) and references therein.

6. SILICATE DUST IN THE DIFFUSE MEDIUM OF THE MILKY WAY AND OTHER GALAXIES

Dust grains, freshly formed in the winds of AGB stars and supergiants, are ejected into the ISM where rapid mixing occurs. Dust cycles between the denser cloud phases and the intercloud medium, gets destroyed by strong supernova shocks, possibly reforms in the ISM and gets incorporated in newly born stars (Dorschner & Henning 1995; Draine 2003, 2010). Most of the

available Si, Mg, and Fe should be tied up in the form of cosmic dust (Mathis 1998). There is no evidence for other interstellar Si-bearing dust components (e.g., SiC) nor for interstellar Fe or Mg oxides, indicating that most of these metals are consumed by silicates, although free Fe particles may exist (Whittet et al. 1997, Chiar & Tielens 2006). Several abundance studies tried to constrain the (Fe+Mg)/Si ratio in interstellar silicates. Sofia & Meyer (2001) concluded that this ratio is close to 2:1, indicating that the grains have a composition similar to $(Mg,Fe)SiO_4$. A new tool to analyze the elemental composition of cosmic silicates is provided by X-ray spectroscopy. Costantini, Freyberg & Predehl (2005) observed the X-ray halo of the bright X-ray binary Cyg X-2 and found evidence for silicates with olivine- and pyroxene-type composition. Their best-fit models required a certain amount of Fe locked in silicates with Mg/Fe ratios of about 5:2. This would imply that only half of the available Fe is locked in silicates and the rest must be in other compounds.

Silicate dust in the diffuse ISM, in molecular clouds, and in HII regions is generally characterized by smooth absorption profiles peaking at about 9.7 and 18 μm, which can be identified by amorphous Fe-Mg silicates. The silicates in the diffuse ISM have been probed along different lines of sight, including the Galactic center (e.g., Lutz et al. 1996), the B-type hypergiant star Cygnus OB2 No. 12 (e.g., Whittet et al. 1997; Bowey, Rawlings & Adamson 2004), and a variety of Wolf-Rayet stars (Roche & Aitken 1984, Chiar & Tielens 2006). The 10-μm absorption profiles are quite similar to that of the red supergiant μ Cep, indicating some compositional and structural similarity in the silicates (Chiar & Tielens 2006). Apart from these compositional and structural similarities, conclusions about the "genetic" relations between these different dust components should not be drawn.

In the case of galactic center sources, contributions from local molecular cloud dust to the absorption profile and blending of emission and absorption features occur, making the interpretation of these data in terms of "pure" interstellar silicates more of a challenge.

In the ISO spectrum along the line of sight to Cygnus OB2 No. 12, Whittet et al. (1997) found an indication for a shallow absorption feature at 2.75 μm, which they interpreted as being caused by phyllosilicates. They discussed a variety of mechanisms to produce hydrous silicates in the diffuse ISM, none of which are particularly convincing. In fact, the reality of this shallow feature remains to be demonstrated.

There is considerable absorption in the trough region between the 9.5- and 18-μm features. An interesting candidate as a carrier for this absorption could be alumosilicates, with further evidence coming from the heavy depletion of Al in the ISM (Mutschke et al. 1998, Chiar & Tielens 2006).

Absorption features similar in profile to the features found in our Galaxy have been observed in other heavily obscured galactic nuclei (Roche et al. 2007). Silicate absorption bands have been detected in a variety of IR galaxies, ranging from ultraluminous IR galaxies (e.g., Teplitz et al. 2006, Hao et al. 2007, Sirocky et al. 2008) to a sample of optically invisible high-luminosity galaxies with redshifts between 1.7 and 2.8 (Houck et al. 2005). In the latter case, the silicate features have even been used to determine the redshift of these galaxies. The occurrence of the silicate bands in a wide variety of galaxy environments shows the ubiquity of silicate dust in the Universe.

Absorption profiles in molecular cloud sources and HII regions (Gillett et al. 1975; Willner et al. 1982; Bowey, Adamson & Whittet 1998), including the famous Orion Trapezium profile (Gillett & Forrest 1973), are somewhat broader than the silicate profiles in the diffuse ISM, showing a pronounced long-wavelength wing in the profiles. This wing is indicative of grain growth or absorption by an additional grain component. The Draine & Lee "astronomical" silicate profile does not perfectly fit the observationally based interstellar profiles because they used the Trapezium profile in the 10-μm region and did not constrain the 18-μm profile by observational data (Draine & Lee 1984, Chiar & Tielens 2006; see **Figure 12**).

Figure 12

Interstellar dust absorption profile from Chiar & Tielens (2006) compared to the extinction profile for "astronomical silicates" by Draine & Lee (1984). After Chiar & Tielens (2006).

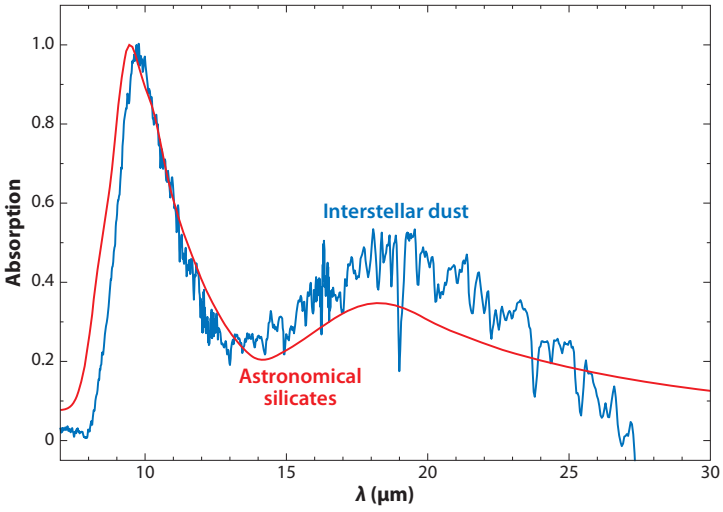

The broad absorption features have only limited diagnostic value in terms of the exact chemical composition of the amorphous interstellar silicates, taking into account that factors such as grain shape and porosity, Mg/Fe ratio, and the polymerization degree of the silicate structure all influence the band profiles. In most of the studies, amorphous silicates with approximately equal amounts of Mg and Fe have been used to represent the interstellar silicate profiles (Draine & Lee 1984; Li & Draine 2001; Kemper, Vriend & Tielens 2004; Chiar & Tielens 2006), although Min et al. (2007, 2008b) argued for very Mg-rich porous silicates as the carrier of the interstellar absorption profiles. However, this result contradicts most of the abundance studies. An interesting additional observational tool to further constrain the composition and structure of cosmic grains is provided by spectropolarimetry in the IR silicate features (Henning & Stognienko 1993).

Bradley (1994) proposed that the so-called GEMS (glass with embedded metal and sulfides) are preserved interstellar silicate grains. GEMS are an abundant component of anhydrous porous interplanetary dust particles (IDPs)—a nonequilibrium assemblage of Mg-rich crystalline silicates (mostly enstatite and forsterite) and amorphous silicates. These IDPs are considered to be the most primitive material in the Solar System, originating from comets. GEMS are submicron-sized particles with numerous small 10- to 50-nm Fe, Fe-Ni, and Fe-Ni sulfide inclusions dispersed in an amorphous Mg-Si-Al-Fe silicate. The sizes and amorphous silicate structure are consistent with those of interstellar silicate grains. In fact, 1%–5% of the GEMS have a nonsolar isotopic composition, indicating a stardust origin (Messenger et al. 2003, Floss et al. 2006). Compositional and spectroscopic arguments have been used to make a case both for or against the hypothesis that most of the GEMS are of interstellar origin (e.g., Bradley & Ishii 2008, Bradley 2010 for a comprehensive discussion).

We note that there is no evidence for the presence of crystalline silicates in the diffuse ISM, with stringent limits of only a few percent of total mass of the silicate dust in crystalline form (Kemper, Vriend & Tielens 2004; Li, Zhao & Li 2007). In view of the finding that AGB stars inject about 15% of their silicates in crystalline form, this seems to be a surprising fact. Amorphization of silicate crystals by low-energy ions produced in supernova shocks (e.g., Jäger et al. 2003b) or high-energy heavy cosmic-ray ions (Bringa et al. 2007) has been discussed for converting crystalline into amorphous silicates with the latter process potentially being more efficient. Extrapolating their experimental results and assuming a cosmic-ray spectrum, Bringa et al. (2007) estimated a lifetime

against amorphization of only 70 million years, much shorter than other relevant timescales. Draine (2010) pointed out that the low crystalline fraction in silicates does not necessarily require that crystals have to be amorphized. The expected grain destruction process in the ISM and the formation of grains in the ISM may suffice to keep the fraction in crystalline silicates low.

In ultraluminous IR galaxies, Spoon et al. (2006) found evidence for crystalline silicates with a mass fraction of about 10%, which is much larger than the upper limit for the dust in the ISM of the Milky Way. They have interpreted this result as evidence for massive stars as a prominent source of crystalline silicates and a lack of amorphization due to cosmic rays in this environment.

7. SILICATES IN GALAXIES WITH ACTIVE GALACTIC NUCLEI

Silicate emission and absorption features attracted much attention in connection with discussions of the AGN unification scheme. Absorption features have been frequently observed in the spectra of type II AGN (Roche et al. 1991, Hao et al. 2007, Zakamska et al. 2008). Type II AGN do not show evidence for high-velocity gas in optical spectra. In the AGN unification scheme, these systems are assumed to be seen edge-on and most of the central regions are obscured by large amounts of dust in the molecular torus. In type I AGN, we see the high-velocity gas component of the broad-line region because the galaxies are tilted toward us. Here we should see silicate features in emission coming from the hot surface of the inner torus wall (Pier & Krolik 1993). Unexpectedly, the feature was never seen in emission before the *Spitzer* mission. In order to solve this puzzle, several proposals have been made, including models with different grain properties and severe modifications of the torus model (see Schartmann et al. 2008 and references therein).

Meanwhile, silicate emission features were found with *Spitzer* spectroscopy in galaxies with different AGN activity, ranging from very luminous quasars (Hao et al. 2005, Siebenmorgen et al. 2005) down to lower-luminosity type I Seyfert galaxies and LINERs (Sturm et al. 2005, Hao et al. 2007, Thompson et al. 2009; see **Figure 13**). Although this finding seems to be in agreement with the expected emission from the torus walls, the derived low dust temperatures are inconsistent with hot dust emission. Furthermore, not all type I AGN show silicate emission profiles. This favors an explanation where the silicate emission does not come from the hot torus walls, but from an extended region of optically thin emission. In addition, emission features were also detected in type 2 quasars and interpreted as emission coming from the narrow-line region (Schweitzer et al. 2008). However, Mason et al. (2009) noted that emission features could also be produced in

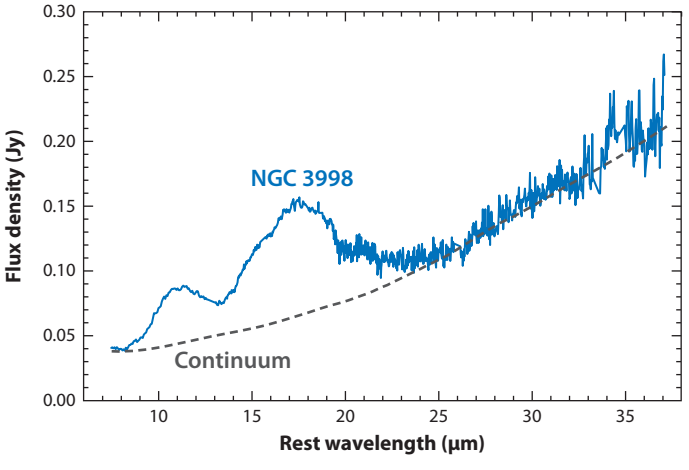

Figure 13

Spitzer spectrum of the type 1 LINER galaxy NGC 3998, showing silicate features in emission. After Sturm et al. (2005).

edge-on clumpy torus models. This discussion shows how important silicate features can be as an analytic tool for constraining the dust distribution in AGNs and quasars.

We note that the 10-μm profiles of the quasar and AGN spectra are often different from "standard" ISM dust in our Galaxy, indicating different composition, size distribution, porosity, or degree of crystallinity (e.g., Li, Shi & Aigen 2008; Raban et al. 2009).

Mid-IR interferometry with the VLTI is now contributing to our knowledge of the dust properties in galaxies with active nuclei (Jaffe et al. 2004, Tristram et al. 2007, Raban et al. 2009). In the type II Seyfert galaxy NGC 1068, Jaffe et al. (2004) and Raban et al. (2009) found that the silicate absorption profile, produced in the molecular torus, is different from standard ISM galactic dust. In the case of the Circinus galaxy—a highly inclined galaxy harboring a Seyfert II active nucleus as well as a nuclear starburst—two components could be found (Tristram et al. 2007). A smaller and dense disk region is seen at high inclination and seems to show the silicate feature in emission. It is surrounded by a larger torus that gives rise to a very strong silicate absorption feature. In this case the silicate absorption profile is very similar to standard galactic ISM dust with not much evidence for processing.

8. SUMMARY AND OUTLOOK

IR spectroscopy, especially from the ISO and *Spitzer* missions, has provided a very rich database on the nature of cosmic silicates. Amorphous and crystalline silicates could be identified in a large variety of environments. Systematic and comparative studies of the silicate spectra will allow a better understanding of the life cycle of this material. The availability of adequate laboratory data on cosmic silicate dust analogs was a necessary prerequisite for the analysis of the astronomical data. The study of silicates in protoplanetary disks has emerged as a rich research field, providing important information on dust evolution and transport processes in disks. Observations of silicates can be used to determine redshifts in high-z objects and to help researchres understand the morphology of AGNs.

The much increased sensitivity of the *James Webb Space Telescope* will allow researchers to get high-quality IR spectra of much fainter objects than presently investigated. Higher spatial resolution with mid-IR instruments on the next generation of extremely large telescopes and long-baseline mid-IR interferometry will lead to a better understanding of silicate formation and evolution in circumstellar outflows of evolved stars and protoplanetary and debris disks.

With the launch of the *Herschel Space Observatory*, the far-IR spectral window for the characterization of cosmic silicates has been opened. In the *Herschel* wavelength range, solid-state features due to lattice vibrations of heavy ions or ion groups with low binding energies can be expected to occur. In addition, phonon-difference processes will contribute to the continuum emission, but will rarely lead to well-defined bands. A prominent feature of forsterite, observed with ISO in a few very bright IR sources, is located around 69 μm. This feature is the best tracer of Mg-rich olivines. In addition, its band position can be used as an independent measure of the dust temperature (e.g., Koike et al. 2006). Diopside, not conclusively identfied in *Spitzer* data of protoplanetary disks, has a prominent far-IR feature at 65–66 μm (Koike et al. 2000). Evidence for the presence of hydrous silicates outside the Solar System remain so far illusive. Hydrous silicates are among the minerals with the most pronounced far-IR bands, and *Herschel* data will clarify the presence of this material in space. Laboratory experiments show that hydrous silicates have various bands between 50 and 300 μm with exact positions and widths depending on temperature (Mutschke et al. 2008). Additional laboratory data at these wavelengths at a variety of temperatures are needed to allow a deeper understanding of *Herschel* observations.

DISCLOSURE STATEMENT

The author is not aware of any affiliations, memberships, funding, or financial holdings that might be perceived as affecting the objectivity of this review.

ACKNOWLEDGMENTS

I thank Johann Dorschner, Joachim Gürtler, Friedrich Huisken, Cornelia Jäger, and Harald Mutschke (all Jena), Jeroen Bouwman (Heidelberg), and Rens Waters (Amsterdam) for many years of exciting collaborative research on cosmic silicates and their analogs in the laboratory. I am particularly thankful to Cornelia Jäger and Joe Carson for critically reading the review. I thank Jean Chiar (Mountain View), Hans-Peter Gail (Heidelberg), and Eckhard Sturm (Garching) for providing figures for this review.

LITERATURE CITED

Ábrahám P, Juhász A, Dullemond CP, Kóspál Á, van Boekel R, et al. 2009. *Nature* 459:224–26
Apai D, Lauretta DS, eds. 2010. *Protoplanetary Dust—Astrophysical and Cosmochemical Perspectives*. Cambridge: Cambridge Univ. Press
Apai D, Pascucci I, Bouwman J, Natta A, Henning Th, Dullemond CP. 2005. *Science* 310:834–36
Beichman CA, Bryden G, Gautier TN, Stapelfeldt KR, Werner MW, et al. 2005. *Ap. J.* 626:1061–69
Bockelée-Morvan D, Gautier D, Hersant F, Huré J-M, Robert F. 2002. *Astron. Astrophys.* 384:1107–18
Bohren CF, Huffman DR. 1983. *Absorption and Scattering of Light by Small Particles*. New York: Wiley
Boudet N, Mutschke H, Nayral C, Jäger C, Bernard J-P, et al. 2005. *Ap. J.* 633:272–81
Bouwman J, de Koter A, Dominik C, Waters LBFM. 2003. *Astron. Astrophys.* 401:577–92
Bouwman J, Henning Th, Hillenbrand LA, Meyer MR, Pascucci I, et al. 2008. *Ap. J.* 683:479–98
Bouwman J, Meeus G, de Koter A, Hony S, Dominik C, Waters LBFM. 2001. *Astron. Astrophys.* 375:950–62
Bouwman J, Lawson WA, Juhász A, Dominik C, Feigelson ED, et al. 2010. *Ap. J.* Submitted
Bowey JE, Adamson AJ, Whittet DCB. 1998. *MNRAS* 298:131–38
Bowey JE, Lee C, Tucker C, Hofmeister AM, Ade PAR, Barlow MJ. 2001. *MNRAS* 325:886–96
Bowey JE, Rawlings MG, Adamson AJ. 2004. *MNRAS* 348:L13–17
Bradley JP 1994. *Science* 265:925–29
Bradley JP. 2010. See Henning 2010. In press
Bradley JP, Ishii HA. 2008. *Astron. Astrophys.* 486:781–84
Bringa EM, Kucheyev SO, Loeffler MJ, Baragiola RA, Tielens AGGM, et al. 2007. *Ap. J.* 662:372–78
Brucato JR, Colangeli L, Mennella V, Palumbo P, Bussoletti E. 1999. *Astron. Astrophys.* 348:1012–19
Brucato JR, Strazzulla G, Baratta G, Colangeli L. 2004. *Astron. Astrophys.* 413:395–401
Carpenter JM, Bouwman J, Mamajek EE, Meyer MR, Hillenbrand LA, et al. 2009. *Ap. J. Suppl. Ser.* 181:197–226
Chen CH, Li A, Bohac C, Kim KH, Watson DM, et al. 2007. *Ap. J.* 666:466–74
Chiar JE, Tielens AGGM. 2006. *Ap. J.* 637:774–85
Clayton DD, Nittler LR. 2004. *Annu. Rev. Astron. Astrophys.* 42:39–78
Cohen M, Witteborn FC. 1985. *Ap. J.* 294:345–56
Colangeli L, Henning Th, Brucato JR, Clément D, Fabian D, et al. 2003. *Astron. Astrophys. Rev.* 11:97–152
Costantini E, Freyberg MJ, Predehl P. 2005. *Astron. Astrophys.* 444:187–200
Crovisier J, Leech K, Bockelée-Morvan D, Brooke TY, Hanner MS, et al. 1997. *Science* 275:1904–7
Demyk K, Carrez Ph, Leroux H, Cordier P, Jones AP, et al. 2001. *Astron. Astrophys.* 368:L38–41
Demyk K, d'Hendecourt L, Leroux H, Jones AP, Borg J. 2004. *Astron. Astrophys.* 420:233–43
Dorschner J, Begemann B, Henning Th, Jäger C, Mutschke H. 1995. *Astron. Astrophys.* 300:503–20
Dorschner J, Henning Th. 1995. *Astron. Astrophys. Rev.* 6:271–333
Draine BT. 2003. *Annu. Rev. Astron. Astrophys.* 41:241–89
Draine BT. 2010. See Henning, Grün & Steinacker 2009, pp. 453–72

Draine BT, Lee HM. 1984. *Ap. J.* 285:89–108
Emery JP, Cruikshank DP, van Cleve J. 2006. *Icarus* 182:496–512
Fabian D, Henning Th, Jäger C, Mutschke H, Dorschner J, Wehrhahn O. 2001. *Astron. Astrophys.* 378:228–38
Fabian D, Jäger C, Henning Th, Dorschner J, Mutschke H. 2000. *Astron. Astrophys.* 364:282–92
Feierberg MA, Witteborn FC, Lebofsky LA. 1983. *Icarus* 56:393–97
Floss C, Stadermann FJ, Bradley JP, Zu Rong Dai, Bajt S, Graham G. 2006. *Geochimica* 70:2371–99
Gail H-P. 2004. *Astron. Astrophys.* 413:571–91
Gail H-P. 2010. See Henning 2010. In press
Gail H-P, Sedlmayr E. 1998. In *The Molecular Astrophysics of Stars and Galaxies*, ed. TW Hartquist, DA Williams, p. 285. Oxford: Clarendon
Gail H-P, Zhukovska SV, Hoppe P, Trieloff M. 2009. *Ap. J.* 698:1136–54
Gervais F, Piriou B. 1975. *Phys. Rev. B* 11:3944–50
Gillett FC, Forrest WJ. 1973. *Ap. J.* 179:483–91
Gillett FC, Forrest WJ, Merrill KM, Soifer BT, Capps RW. 1975. *Ap. J.* 200:609–20
Glauser AM, Güdel M, Watson DM, Henning Th, Schegerer AA, et al. 2009. *Astron. Astrophys.* 508:247–57
Glotch TD, Rossman GR, Aharonson O. 2007. *Icarus* 192:605–22
Gürtler J, Schreyer K, Henning Th, Lemke D, Pfau W. 1998. *Astron. Astrophys.* 346:205–10
Hallenbeck SL, Nuth JA, Daukantas PL. 1998. *Icarus* 131:198–209
Hanner MS, Lynch DK, Russell RW. 1994. *Ap. J.* 425:274–85
Hanner MS, Zolensky ME. 2010. See Henning 2010. In press
Hao L, Spoon HWW, Sloan GC, Marshall JA, Armus L, et al. 2005. *Ap. J.* 625:L75–78
Hao L, Weedman DW, Spoon HWW, Marshall JA, Levenson NA, et al. 2007. *Ap. J.* 655:L77–80
Harker DE, Desch SJ. 2002. *Ap. J.* 565:L109–12
Henning Th, ed. 2003. *Astromineralogy*. Berlin: Springer-Verlag
Henning Th, ed. 2010. *Astromineralogy*. Vol. 815. *Lecture Notes in Physics*. Berlin: Springer-Verlag. 2nd ed.
Henning Th, Grün E, Steinacker J, eds. 2009. *Cosmic Dust—Near and Far*, ASP Conf. Ser. 414. San Francisco: ASP
Henning Th, Il'in VB, Krivova NA, Michel B, Voshchinnikov NV. 1999. *Astron. Astrophys. Suppl. Ser.* 136:405–6
Henning Th, Meeus G. 2010. In *Physical Processes in Circumstellar Disks around Young Stars*, ed. PJV Garcia. Chicago: Chicago Univ. Press. In press
Henning Th, Mutschke H. 1997. *Astron. Astrophys.* 327:743–54
Henning Th, Stognienko R. 1993. *Astron. Astrophys.* 280:609–16
Hofmeister AM, Bowey JE. 2006. *MNRAS* 367:577–91
Houck JR, Soifer BT, Weedman D, Higdon SJU, Higdon JL, et al. 2005. *Ap. J.* 622:L105–8
Jaffe W, Meisenheimer K, Röttgering HJA, Leinert Ch, Richichi A, et al. 2004. *Nature* 429:47–49
Jäger C, Dorschner J, Mutschke H, Posch Th, Henning Th. 2003a. *Astron. Astrophys.* 408:193–204
Jäger C, Fabian D, Schrempel F, Dorschner J, Henning Th, Wesch W. 2003b. *Astron. Astrophys.* 401:57–65
Jäger C, Il'in VB, Henning Th, Mutschke H, Fabian D, et al. 2003c. *J. Quant. Spectr. Rad. Transf.* 79:765–74
Jäger C, Molster FJ, Dorschner J, Henning Th, Mutschke H, Waters LBFM. 1998. *Astron. Astrophys.* 339:904–16
Jones TW, Merrill KM. 1976. *Ap. J.* 209:509–24
Juhász A, Bouwman J, Henning Th, Acke B, van den Ancker ME, et al. 2010. *Ap. J.* In press
Juhász A, Henning Th, Bouwman J, Dullemond CP, Pascucci I, Apai D. 2009. *Ap.J.* 695:1024–41
Kastner JH, Buchanan CL, Sargent B, Forrest WJ. 2006. *Ap. J.* 638:L29–32
Kelley MS, Wooden DH. 2009. *Planet. Space Sci.* 57:1133–45
Kemper F, Vriend WJ, Tielens AGGM. 2004. *Ap. J.* 609:826–37. Erratum 2005. *Ap. J.* 633:534
Kessler-Silacci J, Augereau J-C, Dullemond CP, Geers V, Lahuis F, et al. 2006. *Ap. J.* 639:275–91
Kessler-Silacci JE, Dullemond CP, Augereau J-C, Merín B, Geers VC, et al. 2007. *Ap. J.* 659:680–84
Kimura Y, Miyazaki Yu, Kumamoto A, Saito M, Kaito C. 2008a. *Ap. J.* 680:L89–92
Kimura Y, Sasaki S, Suzuki H, Kumamoto A, Saito M, Kaito C. 2008b. *Ap. J.* 684:1496–501
Knacke RF, Fajardo-Acosta SB, Telesco CM, Hackwell JA, Lynch DK, Russell RW. 1993. *Ap. J.* 418:440–50
Koike C, Chihara H, Tsuchiyama A, Suto H, Sogawa H, Okuda H. 2003. *Astron. Astrophys.* 399:1101–7

Koike C, Mutschke H, Suto H, Naoi T, Chihara H, et al. 2006. *Astron. Astrophys.* 449:583–96
Koike C, Shibai H, Tsuchiyama A. 1993. *MNRAS* 264:654–58
Koike C, Tsuchiyama A, Shibai H, Suto H, Tanabé T, et al. 2000. *Astron. Astrophys.* 363:1115–22
Kotak R, Meikle WPS, Farrah D, Gerardy CL, Foley RJ, et al. 2009. *Ap. J.* 704:306–23
Kozasa T, Hasegawa H, Nomoto K. 1989. *Ap. J.* 344:325–31
Kozasa T, Hasegawa H, Nomoto K. 1991. *Astron. Astrophys.* 249:474–82
Leroux H. 2009. In *Interstellar Dust from Astronomical Observations to Fundamental Studies*, ed. F Boulanger, C Joblin, A Jones, S Madden, pp. 153–69. Les Ulis: EDP Sci.
Li A, Draine BT. 2001. *Ap. J.* 554:778–802
Li MP, Shi QJ, Aigen L. 2008. *MNRAS* 391:L49–53
Li MP, Zhao G, Li A. 2007. *MNRAS* 382:L26–29
Liebau F. 1985. *Structural Chemistry of Silicates*. Berlin: Springer-Verlag
Lisse CM, VanCleve J, Adams AC, A'Hearn MF, Fernández YR, et al. 2006. *Science* 5787:635–40
Lutz D, Feuchtgruber H, Genzel R, Kunze D, Rigopoulou D, et al. 1996. *Astron. Astrophys.* 315:L269–72
Malfait K, Waelkens C, Waters LBFM, Vandenbussche B, Huygen E, de Graauw MS. 1998. *Astron. Astrophys.* 332:L25–28
Mason RE, Levenson NA, Shi Y, Packham C, Gorjian V, et al. 2009. *Ap. J.* 693:L136–40
Mathis JS. 1998. *Ap. J.* 497:824–32
Meeus G, Juhász A, Henning Th, Bouwman J, Chen C, et al. 2009. *Astron. Astrophys.* 497:379–92
Meeus G, Waters LBFM, Bouwman J, van den Ancker ME, Waelkens C, Malfait K. 2001. *Astron. Astrophys.* 365:476–90
Mennella V, Brucato JR, Colangeli L, Palumbo P, Rotundi A, Bussoletti E. 1998. *Ap. J.* 496:1058–66
Merín B, Augereau JC, van Dishoeck EF, Kessler-Silacci J, Dullemond CP, et al. 2007. *Ap. J.* 661:361–67
Messenger S, Keller LP, Lauretta DS. 2005. *Science* 309:737–41
Messenger S, Keller LP, Stadermann FJ, Walker RM, Zinner E. 2003. *Science* 300:105–8
Min M, Dominik C, Hovenier JW, de Koter A, Waters LBFM. 2006. *Astron. Astrophys.* 445:1005–14
Min M, Hovenier JW, Waters LBFM, de Koter A. 2008a. *Astron. Astrophys.* 489:135–41
Min M, Waters LBFM, de Koter A, Hovenier JW, Keller LP, Marckwick-Kemper F. 2007. *Astron. Astrophys.* 462:667–76
Min M, Waters LBFM, de Koter A, Hovenier JW, Keller LP, Marckwick-Kemper F. 2008b. *Astron. Astrophys.* 486:779–80
Molster FJ, Waters LBFM. 2003. See Henning 2003, pp. 121–70
Molster FJ, Waters LBFM, Tielens AGGM. 2002a. *Astron. Astrophys.* 382:222–40
Molster FJ, Waters LBFM, Tielens AGGM, Koike C, Chihara H. 2002b. *Astron. Astrophys.* 382:241–55
Moór A, Apai D, Pascucci I, Ábrahám P, Grady C, et al. 2009. *Ap. J.* 700:L25–29
Mostefaoui S, Hoppe P. 2004. *Ap. J.* 613:L149–52
Murata K, Chihara H, Koike C, Noguchi T, Takakura T, et al. 2009. *Ap. J.* 698:1903–6
Mutschke H, Begemann B, Dorschner J, Gürtler J, Gustafson B, et al. 1998. *Astron. Astrophys.* 333:188–98
Mutschke H, Min M, Tamanai A. 2009. *Astron. Astrophys.* 504:875–82
Mutschke H, Zeidler S, Posch Th, Kerschbaum F, Baier A, Henning Th. 2008. *Astron. Astrophys.* 492:117–25
Nagahara H, Ogawa R, Ozawa K, Tamada S, Tachibana S, Chiba H. 2010. See Henning, Grün & Steinacker 2009, pp. 403–10
Natta A, Meyer MR, Beckwith SVW. 2000. *Ap. J.* 534:838–45
Nguyen AN, Stadermann FJ, Zinner E, Stroud RM, Alexander CM O'D, Nittler LR. 2007. *Ap. J.* 656:1223–40
Nozawa T, Kozasa T, Habe A, Dwek E, Umeda H, et al. 2007. *Ap. J.* 666:955–66
Olofsson J, Augereau J-C, van Dishoeck EF, Merín B, Lahuis F, et al. 2009. *Astron. Astrophys.* 507:327–45
Ossenkopf V, Henning Th, Mathis JS. 1992. *Astron. Astrophys.* 261:567–78
Pascucci I, Apai D, Luhman K, Henning Th, Meyer MR, et al. 2009. *Ap. J.* 696:143–59
Pier EA, Krolik JH. 1993. *Ap. J.* 418:673–86
Raban D, Jaffe W, Röttgering H, Meisenheimer K, Tristram KRW. 2009. *MNRAS* 394:1325–37
Ratzka Th, Leinert C, Henning Th, Bouwman J, Dullemond CP, Jaffe W. 2007. *Astron. Astrophys.* 471:173–85
Rho J, Reach WT, Tappe A, Hwang U, Slavin JD, et al. 2009. *Ap. J.* 700:579–96

Rietmeijer FJM. 2009. *Ap.J.* 705:791–97
Roche PF, Aitken DK. 1984. *MNRAS* 208:481–92
Roche PF, Aitken DK, Smith CH, Ward MJ. 1991. *MNRAS* 248:606–29
Roche PF, Packham C, Aitken DK, Mason RE. 2007. *MNRAS* 375:99–104
Sargent BA, Forrest WJ, Tayrien C, McClure MK, Li A, et al. 2009. *Ap. J.* 690:1193–207
Schartmann M, Meisenheimer K, Camenzind M, Wolf S, Tristram KRW, Henning Th. 2008. *Astron. Astrophys.* 482:67–80
Schweitzer M, Groves B, Netzer H, Lutz D, Sturm E, et al. 2008. *Ap. J.* 679:101–17
Servoin JL, Piriou B. 1973. *Phys. Status Solidi B* 55:677–86
Sicilia-Aguilar A, Hartmann LW, Watson D, Bohac C, Henning Th, Bouwman J. 2007. *Ap. J.* 659:1637–60
Siebenmorgen R, Haas M, Krügel E, Schulz B. 2005. *Astron. Astrophys.* 436:L5–8
Sirocky MM, Levenson NA, Elitzur M, Spoon HWW, Armus L. 2008. *Ap. J.* 678:729–43
Sloan GC, Devost D, Bernard-Salas J, Wood PR, Houck JR. 2006. *Ap. J.* 638:472–77
Sloan GC, Kraemer KE, Wood PR, Zijlstra AA, Bernard-Salas J, et al. 2008. *Ap. J.* 686:1056–81
Sofia UJ, Meyer DM. 2001. *Ap. J.* 554:L221–24. Erratum. 2001. *Ap. J.* 558:L147
Sogawa H, Koike C, Chihara H, Suto H, Tachibana S, et al. 2006. *Astron. Astrophys.* 451:357–61
Spitzer WG, Kleinmann DA. 1961. *Phys. Rev.* 121:1324–35
Spoon HWW, Tielens AGGM, Armus L, Sloan GC, Sargent B, et al. 2006. *Ap. J.* 638:759–65
Sturm E, Schweitzer D, Lutz D, Contursi A, Genzel R, et al. 2005. *Ap. J.* 629:L21–23
Suto H, Koike C, Sogawa H, Tsuchiyama A, Chihara H, Mizutani K. 2002. *Astron. Astrophys.* 389:568–71
Suto H, Sogawa H, Tachibana S, Koike C, Karoji H, et al. 2006. *MNRAS* 370:1599–606
Teplitz HI, Armus L, Soifer BT, Charmandaris V, Marshall JA, et al. 2006. *Ap. J.* 638:L1–4
Thompson GD, Levenson NA, Uddin SA, Sirocky MM. 2009. *Ap. J.* 697:182–93
Thompson SP. 2008. *Astron. Astrophys.* 484:251–65
Tristram KRW, Meisenheimer K, Jaffe W, Schartmann M, Rix HW, et al. 2007. *Astron. Astrophys.* 474:837–50
van Boekel R, Min M, Leinert Ch, Waters LBFM, Richichi A, et al. 2004. *Nature* 432:479–82
van Boekel R, Min M, Waters LBFM, de Koter A, Dominik C, et al. 2005. *Astron. Astrophys.* 437:189–208
van Boekel R, Waters LBFM, Dominik C, Bouwman J, de Koter A, et al. 2003. *Astron. Astrophys.* 400:L21–24
van den Ancker ME, Bouwman J, Wesselius PR, Waters LBFM, Dougherty SM, van Dishoeck EF. 2000. *Astron. Astrophys.* 357:325–29
Vollmer C, Brenker FE, Hoppe P, Stroud RM. 2009. *Ap. J.* 700:774–82
Vollmer C, Hoppe P, Brenke FE. 2008. *Ap. J.* 684:611–17
Voors RHM, Waters LBFM, Morris PW, Trams NR, de Koter A, Bouwman J. 1999. *Astron. Astrophys.* 341:L67–70
Voshchinnikov NV, Henning Th. 2008. *Astron. Astrophys.* 483:L9–12
Voshchinnikov NV, Il'in VB, Henning Th, Dubkova DN. 2006. *Astron. Astrophys.* 445:167–77
Wang LM, Miller ML, Ewing RC. 1993. *Ultramicroscopy* 51:339–47
Waters LBFM, Beintema DA, Zijlstra AA, de Koter A, Molster FJ, et al. 1998a. *Astron. Astrophys.* 331:L61–64
Waters LBFM, Cami J, de Jong T, Molster FJ, van Loon JTh, et al. 1998b. *Nature* 391:868–71
Waters LBFM, Molster FJ, de Jong T, Beintema DA, Waelkens C, et al. 1996. *Astron. Astrophys.* 315:L361–64
Watson DM. 2010. See Henning, Grün & Steinacker 2009, pp. 77–98
Watson DM, Leisenring JM, Furlan E, Bohac CJ, Sargent B, et al. 2009. *Ap. J. Suppl. Ser.* 180:84–101
Wehrstedt M, Gail H-P. 2002. *Astron. Astrophys.* 385:181–204
Whittet DCB, Boogert ACA, Gerakines PA, Schutte W, Tielens AGGM, et al. 1997. *Ap. J.* 490:729–34
Willner SP, Gillett FC, Herter TL, Jones B, Krassner J, et al. 1982. *Ap. J.* 253:174–87
Wooden DH. 2008. *Space Sci. Rev.* 138:75–108
Woolf NJ, Ney EP. 1969. *Ap. J.* 155:L181–84
Yamamura I, Dominik C, de Jong T, Waters LBFM, Molster FJ. 2000. *Astron. Astrophys.* 363:629–39
Zakamska NL, Gomez L, Strauss MA, Krolik JH. 2008. *Ap. J.* 136:1607–22
Zijlstra AA, Matsuura M, Wood PR, Sloan GC, Lagadec E, et al. 2006. *MNRAS* 370:1961–78
Zolensky ME, Zega ThJ, Yano H, Wirick S, Westphal A, et al. 2006. *Science* 314:1735–39